Efficient partitioning schemes for fluid–structure interaction problems

R. K. Singh,* T. Kant† and A. Kakodkar*
**Reactor Engineering Division, Bhabha Atomic Research Centre, Trombay, Bombay 400 085, India*
†Department of Civil Engineering, Indian Institute of Technology, Powai, Bombay 400 076, India
(Received August 1989)

ABSTRACT

This paper demonstrates the capability of staggered solution procedure for coupled fluid–structure interaction problems. Three possible computational paths for coupled problems are described. These are critically examined for a variety of coupled problems with different types of mesh partitioning schemes. The results are compared with the reported results by continuum mechanics priority approach—a method which has been very popular until recently. Optimum computational paths and mesh partitionings for two field problems are indicated. Staggered solution procedure is shown to be quite effective when optimum path and partitionings are selected.

INTRODUCTION

Fluid–structure interaction has become an important research and development activity in recent years for nuclear, space and offshore industries. The topic merits special consideration in the area of nuclear reactor safety in a number of situations. The important applications are design and analysis of liquid containers against earthquakes, design of vapour suppression pool for loss of coolant accident and studies of submerged components for postulated accident condition giving rise to pressure transients in fluid. There are two approaches available to analyse a fluid–structure interaction problem. In the first approach an existing structure dynamics code is modified to make the shear modulus zero in the fluid domain. The fluid–structure interface is constrainted to have normal displacement continuity[5,7,8,19,20]. An optimum penalty parameter or irrotational flow condition is enforced to avoid any spurious circulation mode or zero energy mode. In this formulation either contact elements are used at fluid–structure interface or a penalty parameter is selected for suppressing these spurious modes. Au-Yang[1] defines this method as structure mechanics priority or continuum mechanics approach.

The second approach is based on coupled solution of acoustic wave equation and structure dynamics equation by method of partitioning[2–4,18] using staggered solution scheme. The advantages of this approach are that it is modular in nature, various types of mesh and field partitionings are possible and a variety of linear or non-linear coupled fluid–structure interaction problems can be solved. In the case of an acoustic medium interacting with structure, this approach results in considerable saving in terms of number of degree of freedom for the fluid domain. For example, in the pressure formulation only one variable is assigned at each node for two- or three-dimensional problems. The limitations of this method are as follows. The resulting equations are unsymmetric. So iterative schemes are required for solution of equations of two fields. The fluid and structure responses have to be corrected due to interaction term, until the convergence is met. The coupling at fluid–structure interface causes a large bandwidth. However, this limitation can be overcome by using skyline storage scheme and independent equation numbering system at the interface[18].

Belytschko[13] has classified transient problems in two categories, wave propagation problems and inertial problems. In wave propagation problem, accuracy of wave front resolution is important, so high vibration modes also have to be integrated properly. In case of inertial problems, the response lies in few lower modes, so higher modes are not important and they must be filtered out. In the case of fluid–structure interaction problem one is faced with both types of situations. Normally in fluid domain the pressure wave has to be traced with accuracy if it is likely to excite significant structure modes strongly. Another important consideration for fluid–structure interaction problems is selection of optimum integrator. Two methods are available: explicit method and implicit method. It is well known that an explicit scheme is conditionally stable, thus limiting the time step size. But this method requires less CPU time and small storage since it does not call for solution of system of simultaneous equations. On the other hand, implicit scheme requires solution of system of equations at each time step. This method is unconditionally stable and larger time steps are permitted depending

0264–4401/90/020101–15$2.00

on the order of accuracy required. Errors in numerical solution process are introduced by spatial discretization and temporal discretization in the transient problems. Normally higher modes are in error, but by selection of a proper integrator, time step and artificial damping, optimum results can be obtained[13–16,23–25].

The present paper brings out some features of partitioning method for coupled fluid–structure interaction problem. A brief theory is given first. Paul[3] has indicated three computational paths for staggered solution scheme. The details of this are then described. These three paths are critically examined for a variety of coupled problems. It is concluded that selection of optimum path and mesh partitioning is important for efficient solution of coupled problems. Two paths are found to be optimum, the selection of which is governed by type of coupled problem. Numerical studies indicate that the convergence rate of partitioned analysis depends on time step and mesh integrator for fluid and structure along with the path. The paper ends with some conclusions as demonstrated by comparison of the results of present partitioning method with that of continuum mechanics approach[5].

THEORY

The methodology adopted in the present work to analyse a fluid–structure interaction problem is based on the solution of acoustic wave equation by finite elements for fluid domain and analysis of structure based on the displacement method of finite elements. The resulting coupled second-order ordinary differential equations for fluid domain and structure domain are numerically integrated by Newmark's method. The structure normal accelerations are transferred to the fluid domain and fluid pressures are applied to the structure at each time step in an iterative manner. Thus it is possible to solve a purely structure dynamics problem, a purely fluid dynamics problem with homogeneous boundary and a coupled fluid–structure interaction problem by this formulation. Use of Newmark's direct integration method in predictor–multi-corrector form[3,14,15] for the two field equations in an implicit or explicit manner along with sky line storage scheme makes this approach very effective.

Pressure formulation for fluid

The governing acoustic wave equation in terms of pressure variable for inviscid, compressible fluid with small displacement is:

$$\nabla^2 p = \frac{1}{c^2}\ddot{p} \qquad \text{(in fluid domain } \Omega_f\text{)} \tag{1}$$

where p is pressure and c is acoustic speed.

The three types of pressure gradients at fluid boundary with outward normal n are:

(i) *Interaction boundary*

$$\Gamma_I \qquad \text{with } p, n = -\rho_f \ddot{u}_n \tag{2}$$

(ii) *Free boundary*

$$\Gamma_F \qquad \text{with } p, n = -\ddot{p}/g \tag{3}$$

(iii) *Radiating boundary*

$$\Gamma_R \qquad \text{with } p, n = -\dot{p}/c \tag{4}$$

Another type of boundary is for prescribed pressure p^s:

$$p = p^s \qquad \text{on } \Gamma_P \tag{5}$$

The above boundaries define the fluid boundary Γ_f completely:

$$\Gamma_f = \Gamma_I + \Gamma_R + \Gamma_F + \Gamma_P \tag{6}$$

Here ρ_f, $\ddot{u}_n$ and g are fluid density, structure normal acceleration at fluid–structure interface and acceleration due to gravity respectively. The above equation (1) along with boundary conditions (2)–(6) result in the following equation after semi-discretization:

$$\mathbf{M}_f\ddot{\mathbf{p}} + \mathbf{C}_f\dot{\mathbf{p}} + \mathbf{K}_f\mathbf{p} = \rho_f\mathbf{Q}_f(\ddot{\mathbf{u}} + \ddot{\mathbf{u}}_g) + \mathbf{f}_f \tag{7}$$

where $\mathbf{M}_f$, $\mathbf{C}_f$ and $\mathbf{K}_f$ are fluid mass, damping and stiffness matrices respectively. $\mathbf{Q}_f$ couples the fluid equations to structure and ground acceleration vectors $\ddot{\mathbf{u}}$ and $\ddot{\mathbf{u}}_g$ respectively and $\mathbf{f}_f$ is fluid force vector.

Structural dynamics problem

The semi-discrete structural dynamics equation for a structure coupled with an acoustic medium of above description is:

$$\mathbf{M}_s\ddot{\mathbf{u}} + \mathbf{C}_s\dot{\mathbf{u}} + \mathbf{K}_s\mathbf{u} = \mathbf{f}_s - \mathbf{M}_s\ddot{\mathbf{u}}_g + \mathbf{Q}_s\mathbf{p} \tag{8}$$

where $\mathbf{M}_s$, $\mathbf{C}_s$ and $\mathbf{K}_s$ are structure mass, damping and stiffness matrices respectively. $\mathbf{u}, \dot{\mathbf{u}}, \ddot{\mathbf{u}}$ are structure displacement, velocity and acceleration respectively. $\mathbf{Q}_s$ couples the structure equations to fluid pressure. It is easily recognized that the coupling matrix $\mathbf{Q}_f = -\mathbf{Q}_s^{\mathrm{T}}$. Appendix I shows forms of various matrices for two domains for two-dimensional problems.

Coupled equation solution strategy

The system of (7) and (8) are coupled second-order ordinary differential equations. Various solution schemes for coupled problems have been suggested by Park and Felippa[2], Paul[3] and Felippa and Geers[4]. The difficulties with field elimination methods are that order of resulting differential equation is higher, sparseness of matrices are lost and special algorithms are required due to new initial conditions. The method of simultaneous solutions also poses some computational difficulties. The resulting equations are unsymmetric (as seen by (7) and (8)). Attempts to make them symmetric leads to loss in bandedness of the resulting equations[3]. The method of partitioning overcomes the above mentioned limitations. Here the structure or the fluid field may be integrated by implicit, explicit or mixed time integration scheme on two different meshes in a staggered fashion and interaction effect can also be accounted.

Since in most of the problems the critical time step for the two fields may be of varying magnitude, it is desirable to use implicit (I), explicit (E) or mixed explicit–implicit (E–I) time integration scheme either for one field or for both the fields. In the present case the predictor–multi-corrector algorithm due to Hughes[14] is used. This is based on elementwise splitting of mesh in implicit and explicit form which is described in Appendix II. It has been used by Paul[3] for coupled fluid–structure interaction problems, where three possible computational paths are described. In path 1 the field variables for both the fields are predicted and the predicted variables at the interaction boundary are transferred to the respective fields. Both fields are solved with predicted interaction variable simultaneously. In path 2 the sequence is structure then fluid, i.e. predicted pressure is applied to the structure and the corrected structure response after solution of the structure equations is transferred to the fluid to take into account the interaction effect. Path 3 is just opposite to path 2 where the sequence is first fluid then structure.

The stability analysis of single field Newmark integrator is well established[13,14,16]. Hughes[14] has also established the stability criteria in single fields with explicit–implicit partitioning. It has been proved that mesh partitioning for single field problem is quite effective. Stiff elements could be treated implicitly while flexible elements could be treated explicitly without affecting stability. Time step for such partitioning depends on minimum period of explicit mesh alone. Coupled problems with various mesh partitioning schemes along with the predictor–multi-corrector algorithm are not easily amenable to stability analysis. Some general notions are available in References 2–4, where it is concluded that stability depends on integrator, mesh partition, predictor formula and computational path. The major difficulty with this is that modal equations are not available in explicit form and the order of characteristic polynomial for such an analysis is large. However, it is realized that based on information available, stable algorithms can be selected and optimum mesh partitioning is possible. It is also obvious that out of the three paths described above best path will be either 2 or 3 depending on type of problem; this is discussed in the next section. Path 1 obviously is not recommended as it gives slower convergence and becomes unstable or sometimes gives convergence problems. Satisfactory convergence is the major goal which is achieved by effective mesh partitioning and selection of optimum computational path.

CASE STUDIES

To study the performance of present formulation and to examine the effects of various mesh partitioning and computational paths, a number of problems were analysed with code FLUSOL[18] developed by the authors. This can be used to solve two-dimensional plane stress–plane strain and axisymmetric problems of fluid–structure interaction. The present results were obtained by staggered solution schemes for coupled equation of two fields. The problems have been selected from Akkas[5]. The results reported therein are based on continuum mechanics approach. All the problems were solved by Newmark's explicit or implicit integration scheme in predictor–multi-corrector form with parameters $\beta=0.25$ and $\gamma=0.5$. A tolerance of $1.0E$–05 was used as convergence criteria on the ratio of norm of incremental field variable (pressure or displacement) with norm of total field variable (eqn II.14 of Appendix II). The results reported here were obtained on a Norsk Data machine (ND 560 and ND 570) in double precision.

Pressure wave propagation in a rigid pipe

Figure 1a shows a rigid pipe with a pressure pulse of 1 lb/in^2 applied at one end and the other end is closed. Twenty plane-strain four-noded isoparametric fluid elements were used to discretize the fluid

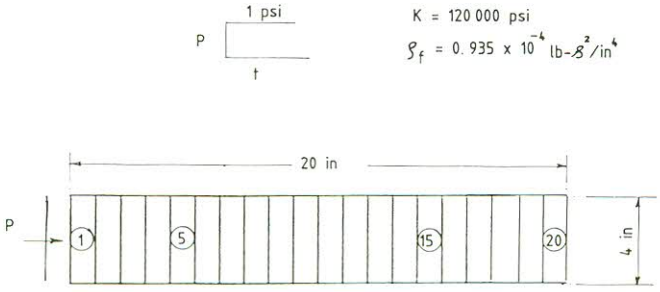

Figure 1a Pressure wave propagation in a pipe

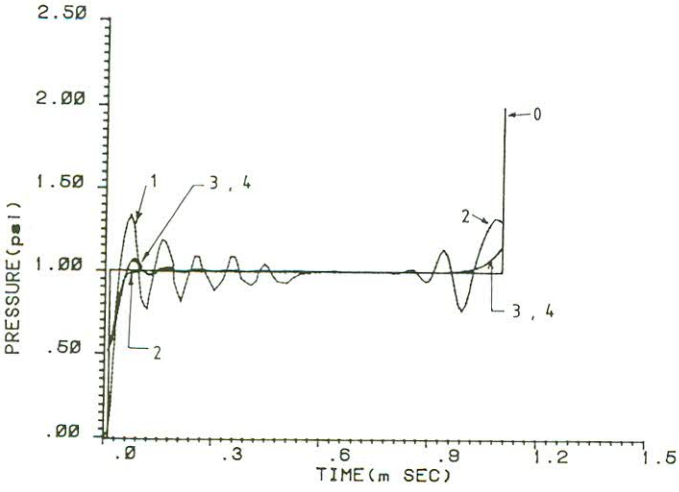

Figure 1b Pressure history in element 1. 0, Exact; 1, Ref. 5; 2, impl. cons.; 3, explicit; 4, impl. lump; $\Delta t = 0.01$ msec

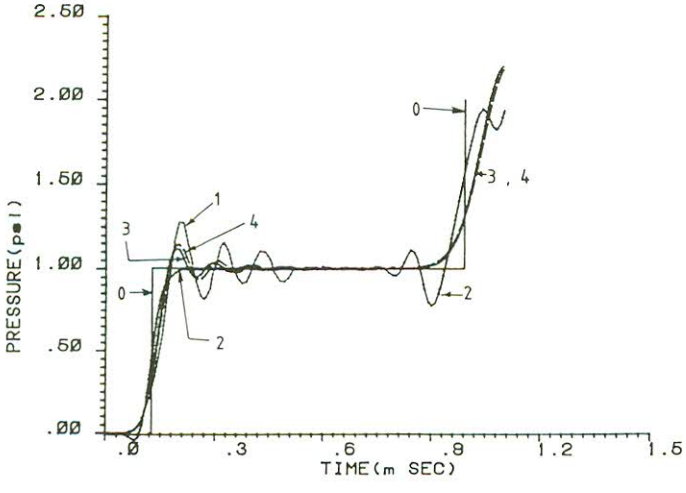

Figure 1c Pressure history in element 5. 0, Exact; 1, Ref. 5; 2, impl. cons.; 3, explicit; 4, impl. lump; $\Delta t = 0.01$ msec

domain. Solution was obtained for single fluid field with homogeneous boundary condition. A time step of 0.01 msec (same as that reported in Reference 5) was used to trace the pressure wave propagation. Results are compared at centre of element 1, 5, 15 and 20 in *Figure 1b–1e*, by interpolating the pressure history from nodal valves. Three cases namely implicit integration with consistent mass, explicit integration with lumped mass and implicit integration with lumped mass are presented. It ia noted that implicit scheme with consistent mass shows dispersion before the arrival of shock front, while the explicit scheme and implicit scheme with lumped mass show dispersion after the arrival of shock front. This dispersion or oscillatory behaviour at shock front is due to discontinuity, spatial and temporal discretization errors discussed by Schreyer[13]. The present results are better than those in Reference 5 which is based on continuum mechanics approach where pressure is obtained from gradient of nodal displacements.

It has been mathematically established by Hughes[14] that matched methods of time integration, i.e. implicit schemes with consistent mass and explicit scheme with lumped mass represent shock wave accurately. The theoretical argument is that

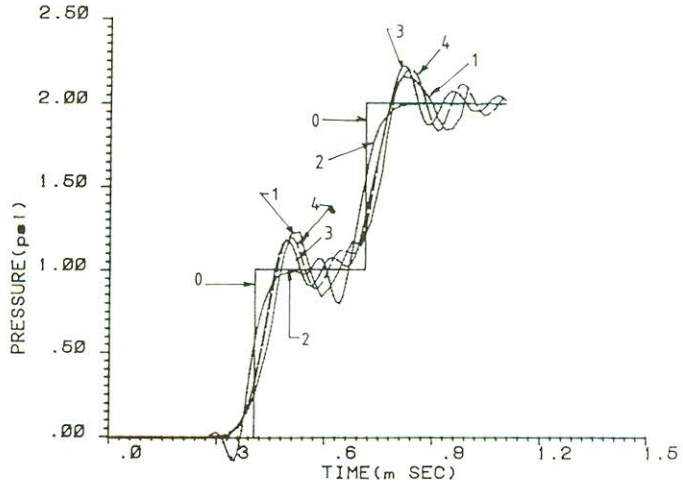

Figure 1d Pressure history in element 15. 0, Exact; 1, Ref. 5; 2, impl. cons.; 3, explicit; 4, impl. lump; $\Delta t = 0.01$ msec

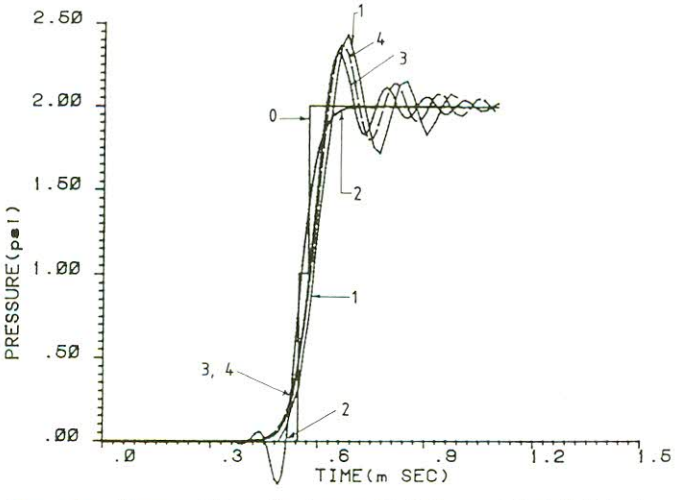

Figure 1e Pressure history in element 20. 0, Exact; 1, Ref. 5; 2, impl. cons.; 3, explicit; 4, impl. lump; $\Delta t = 0.01$ msec

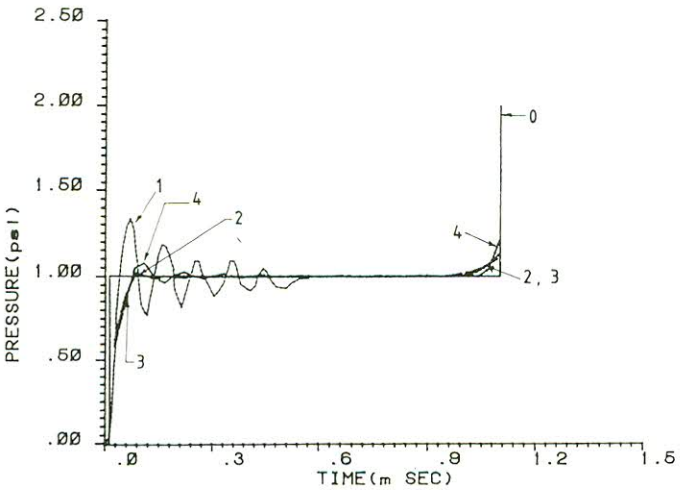

Figure 1f Pressure history in element 1. 0, Exact; 1, Ref. 5; 2, impl. cons.; 3, explicit; 4, impl. lump; $\Delta t = 0.0275$ msec

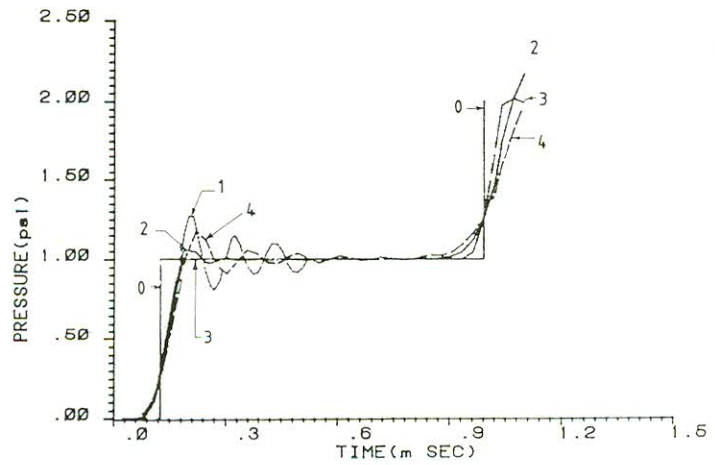

Figure 1g Pressure history in element 5. 0, Exact; 1, Ref. 5; 2, impl. cons.; 3, explicit; 4, impl. lump; $\Delta t = 0.0275$ msec

the spatial and temporal discretization errors tend to cancel each other. The critical time step for this problem is evaluated to be 0.028 msec which is of the order of h/c, where h is the mesh size (1 in) and c is the acoustic speed. Another set of results is presented in *Figures 1f–1i* where a time step of 0.0275 msec (very close to the critical time step) has been used. As expected the accuracy of the explicit method is very good and results show no dispersion. Implicit method with consistent mass shows some oscillations which are either less than or comparable to that reported by Akkas[5]. Implicit method with lumped mass shows oscillations which are either more or comparable with that reported[5]. Thus the present formulation is capable of predicting shock front accurately. The behaviour of implicit and explicit integrator is consistent with the theoretical arguments given by Hughes[14] for shock wave problems.

Plate–fluid interaction problem

Figure 2a shows a fluid reservoir which is closed at one end with a steel plate with fixed ends. A 5×5 mesh of eight-noded isoparametric elements was used for fluid domain. The plate was modelled with 1×5 eight-noded isoparametric plane strain elements. A pressure pulse of 100 kg/cm^2 was applied at one end and pressure history was traced at point A ($X = 142.5$ cm, $Y = 75$ cm) in fluid domain. At first implicit integration with a time step of 0.01 msec was used for fluid and plate. *Figure 2b* shows the results for rigid and flexible plate. Rigid plate solutions are obtained by solving fluid as a single field with homogeneous boundary and also by the coupled solution method with a high Young's modulus of plate (1×10^{19} kg/cm^2). Both approaches give identical results. Again dispersion is noted before the arrival of shock front. For flexible plate case the pressure history is shown to be less

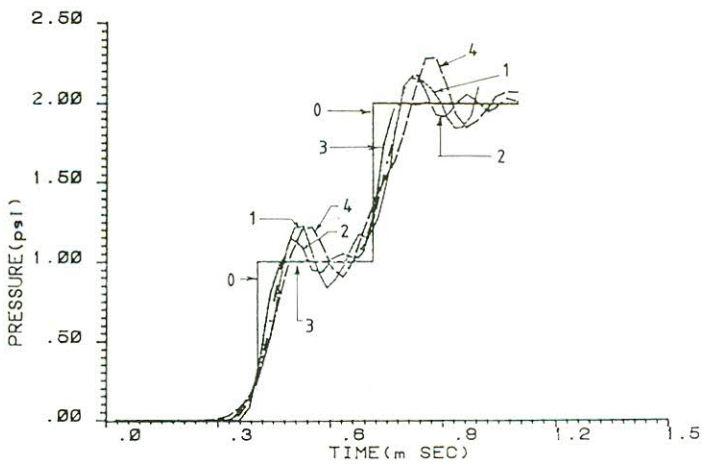

Figure 1h Pressure history in element 15. 0, Exact; 1, Ref. 5; 2, impl. cons.; 3, explicit; 4, impl. lump; $\Delta t = 0.0275$ msec

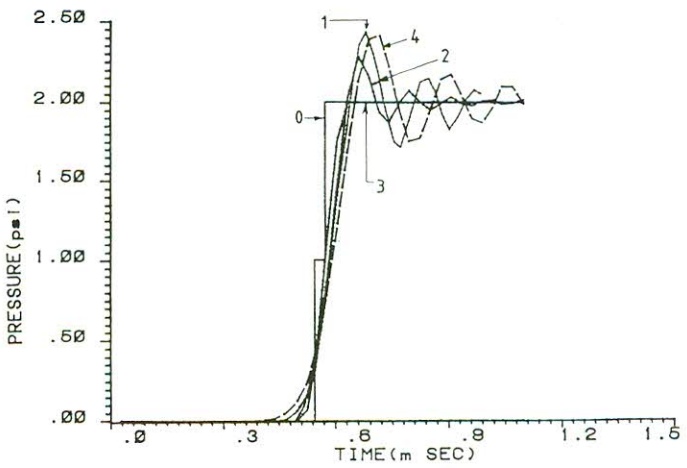

Figure 1i Pressure history in element 20. 0, Exact; 1, Ref. 5; 2, impl. cons.; 3, explicit; 4, impl. lump; $\Delta t = 0.0275$ msec

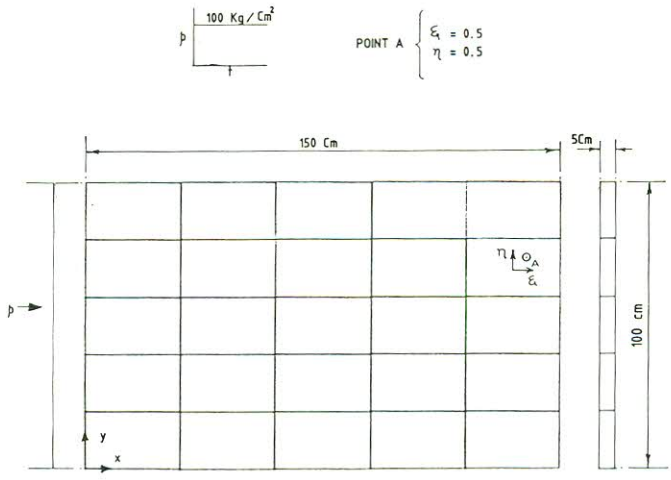

Figure 2a Plate–fluid interaction problem. Reservoir: $C=1.433\times10^5$ cm/sec; $\rho_f=1.019\times10^{-6}$ kg sec^2/cm^4; $g=981$ cm/sec^2. Steel plate: $E=2\times10^6$ kg/cm^2 (flexible), $=1\times10^{19}$ kg/cm^2 (rigid; $\nu=0.3$; $\rho_s=8.002\times10^{-6}$ kg sec^2/cm^2

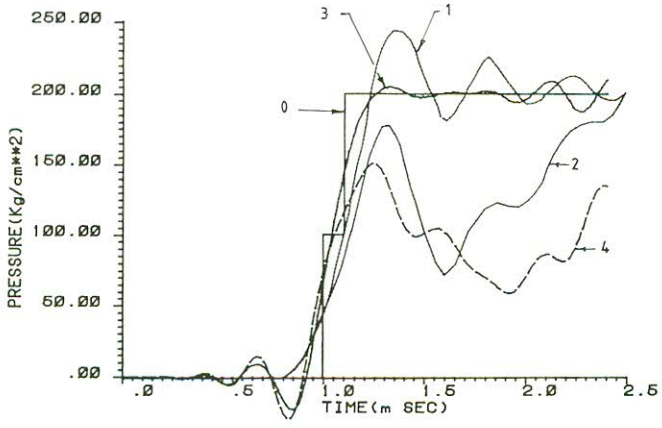

Figure 2b Plate-fluid interaction (8 node). 0, Rigid exact; 1, rigid[5]; 2, flexi.[5]; 3, rigid plate; 4, flexi plate; $\Delta t=0.01$ msec (implicit cons.)

than that reported[5]. Similar observation is made with nine-noded element results in *Figure 2c*. It is noted that single bilinear element across the thickness of plate has been used[5] which is very stiff in bending. The problem was then analysed with 10×10 mesh for fluid and 2×10 mesh for plate with bilinear elements. *Figure 2d* shows the results. Here it is noted that the pressure response is very close to that reported by Akkas[5]. The tendency of pressure curve is to approach the rigid plate solution. Reduced quadrature (1×1) integration for bilinear elements in plate improves the results and pressure response is very close to eight-noded elements result for flexible plate case.

In the present problem with eight-noded elements the smallest time periods for fluid and plate models were evaluated as 0.10914 msec and 6.98×10^{-3} msec respectively. This suggests that fluid field could be solved by explicit method while the plate should be solved by implicit method. *Table 1* shows the smallest time periods for fluid domain for the three models.

The above three problems were solved by treating fluid with explicit integrator while the plate was

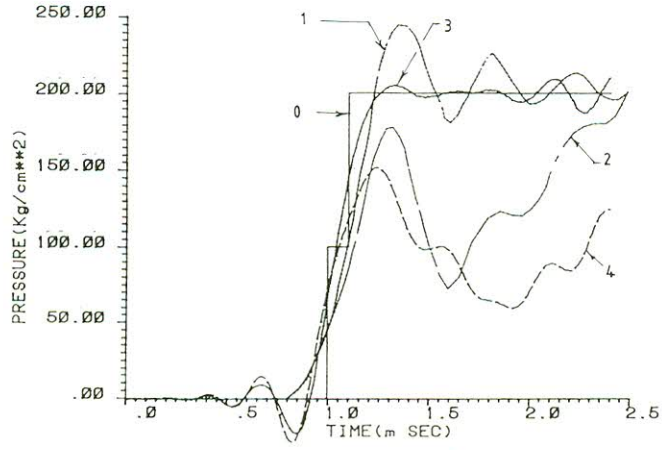

Figure 2c Plate-fluid interaction (9 node). 0, Rigid exact; 1, rigid[5]; 2, flexi.[5]; 3, rigid plate; 4, flexi plate; $\Delta t=0.01$ msec (implicit cons.)

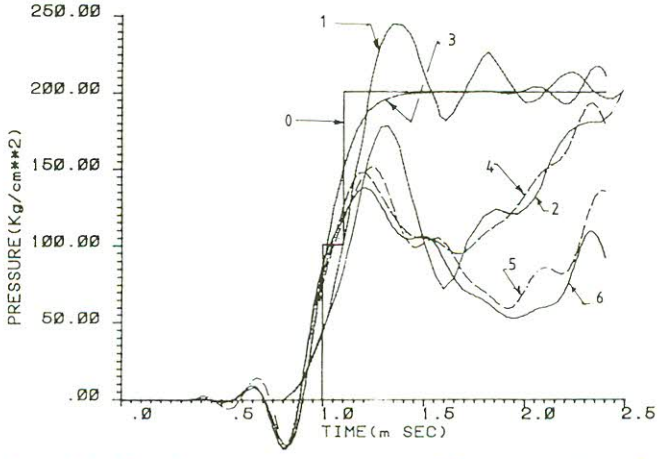

Figure 2d Plate-fluid interaction (4 node). 0, Rigid exact; 1, rigid[5]; 2, flexi.[5]; 3, rigid plate; 4, 2×2 int. flexi; 5, 1×1 int. flexi; 6, 8 node flexi; $\Delta t=0.01$ msec (implicit cons.)

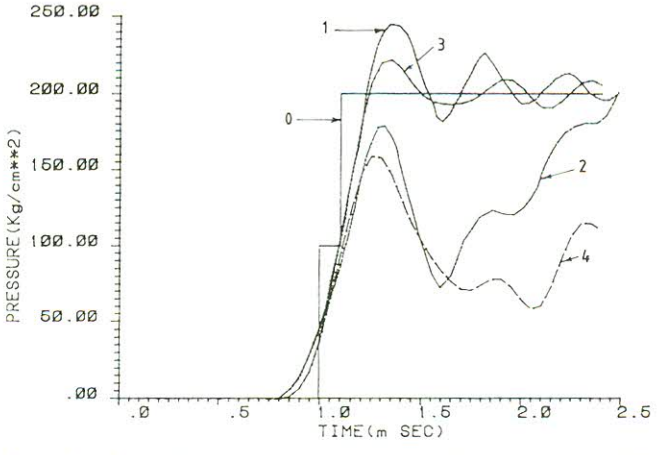

Figure 2e Plate-fluid interaction (9 node). 0, Rigid exact; 1, rigid[5]; 2, flexi.[5]; 3, rigid plate; 4, flexi plate; $\Delta t=0.05$ msec (explicit fluid implicit plate)

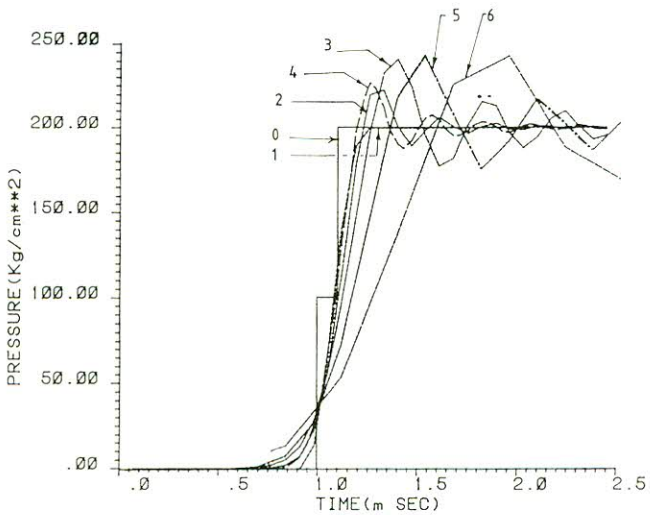

Figure 2f Plate–fluid interaction (4 node) 0, Exact; 1, explicit (Δt_{cr}); 2, impl. cons. (Δt_{cr}); 3, impl. lump. (Δt_{cr}); 4, explicit ($\Delta t_{cr}/2$); 5, implicit ($2\Delta t_{cr}$); 6, implicit ($4\Delta t_{cr}$); $\Delta t_{cr} = 0.07$ msec (uniform mesh)

Table 1 Critical time steps for plate–fluid interaction problem

Smallest period T_{min} (msec)	Eight-noded element	Nine-noded element	Four-noded element
Consistent mass	0.10914	0.0943	0.10563
Lumped mass	0.11376	0.1722	0.22269
$\Delta t_{cr} = T_{min}/\pi$ (msec) →	0.036	0.054	0.07

treated by implicit integrator (*E–I* partitioning). It was realized that in the coupled wave propagation problem *E–I* partitioning for fluid and structure respectively takes a large number of iterations for convergence compared to *I–I* partitioning. This is particularly true at initial steps as shown in *Table 2* for this problem.

From *Table 1* it is noted that the critical time steps for Lagrangian elements are close to the theoretical estimates of h/c and $h/\sqrt{6}c$ for four- and nine-noded elements respectively. The critical time step for eight-noded element is the minimum. So *E–I* partitioning is more effective with Lagrangian elements and bilinear element is the most suitable one. This has been discussed previously[10,13,14] also. *Figure 2e* shows the typical results for *E–I* partitioning with nine-noded elements. The rigid plate solution shows some dispersion after the arrival of shock front even with the explicit integration scheme at a time step very close to the critical time step. This is again attributed to discretization error. Here the critical time step is governed by nodal spacing in the Y direction, while the wave is being traced in the X direction. *Figure 2f* shows results for rigid plate case with four-noded elements in a uniform square mesh (15×10). It is noted that explicit calculation at critical time steps (0.07 msec) shows no dispersion. Implicit calculation at critical time step shows dispersion and it is more in the case of lumped mass than with consistent mass. Results of implicit calculation at twice and four times the critical time steps show large oscillations due to error in higher modes. Explicit results at half the critical time step are also shown, which also shows oscillation due to dispersion.

In the present problem plate vibration is followed by the pressure pulse propagation in fluid, so path 3 is the optimum. The number of iterations per time step is the least for path 3 and maximum for path 1. Path 2 is slightly slower than path 3 in terms of convergence rate. Another important observation about the rate of convergence is for *I–I* partitioning. In this case larger time steps can be used. The number of iterations increases with the time step till 1.0 msec. This is the time required for the pressure wave to reach the plate. Further increase in time step results in reduction in number of iterations again. This is shown in *Table 3* for eight-noded element mesh. At a time step of the order of the time required for the pressure pulse to reach the plate, the numerical behaviour of the fluid model shows a transition from compressible to incompressible fluid case. This results in oscillating response of fluid. Again at still larger time steps the fluid model behaves as purely incompressible and convergence is very rapid. This behaviour is consistent with effect of compressibility for coupled problems[1,2,9,10,13].

Base excitation of water reservoir

The third problem is of a water reservoir of 300 ft × 300 ft size which is excited at the base with a constant acceleration of 1 g (*Figure 3a*). Here fluid boundary is treated to be surrounded by rigid walls. This problem has been studied by Akkas[5] and

Table 2 Number of iterations for plate–fluid interation problem in computational path 3

	Eight-noded element mesh			Nine-noded element mesh		Four-noded element mesh	
	E–I	*E–I*	*I–I*	*E–I*	*I–I*	*E–I*	*I–I*
Δt (msec)	0.030	0.025	0.025	0.05	0.05	0.06	0.06
Average iterations in initial steps →	30–50	15–30	5–6	20–45	5–6	15–27	5–6
Average iterations in latter steps →	15–20	7–10	4–5	8–11	4–5	5–7	4–5

Table 3 Number of iterations in computational path 3 for plate–fluid interaction problem with *I–I* partitioning

	Compressible			Transition			Incompressible		
Time step (msec) →	0.1	0.2	0.35	0.5	1.0	2.0	10.0	100.0	1000.0
Number of iterations	9	11	19	27	46	20	5	3	2

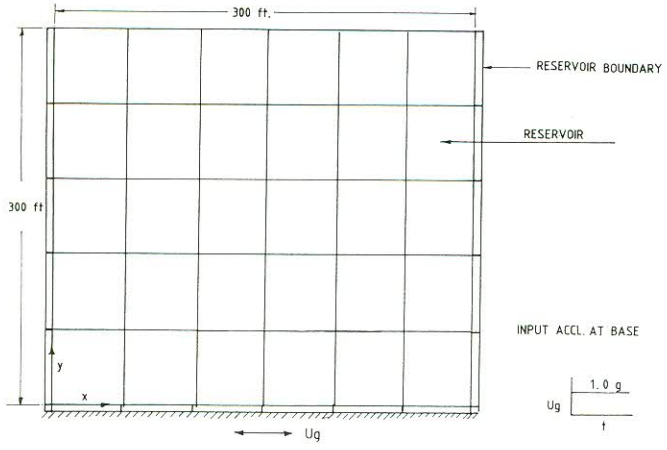

Figure 3a Reservoir with base motion. $C=4720$ ft/sec; $g=32.2$ ft/sec^2; $\rho^f=1.94$ lbs^2/ft^4

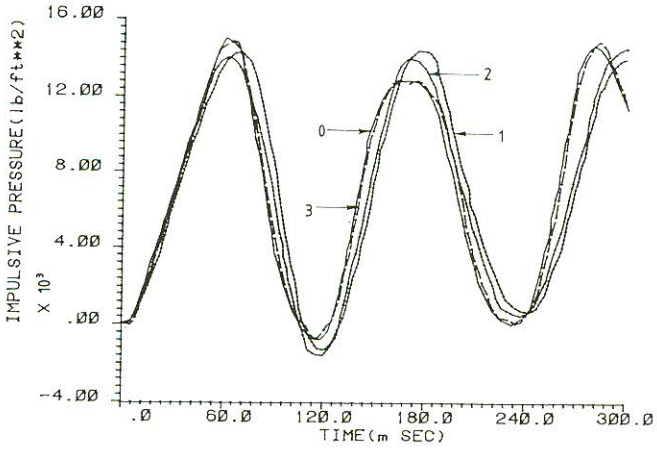

Figure 3c Reservoir under base motion (8 node). 0, Exact; 1, *DI*[5]; 2, *MS*[5]; 3, 8 node; $\Delta t=2.5$ msec (implicit cons.)

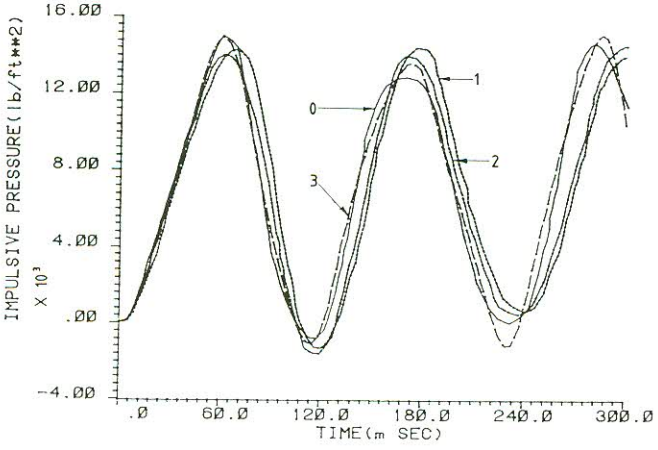

Figure 3b Reservoir under base motion (4 node). 0, Exact[5]; 1, *DI*[5]; 2, *MS*[5]; 3, 4 node; $\Delta t=2.5$ msec (implicit cons.)

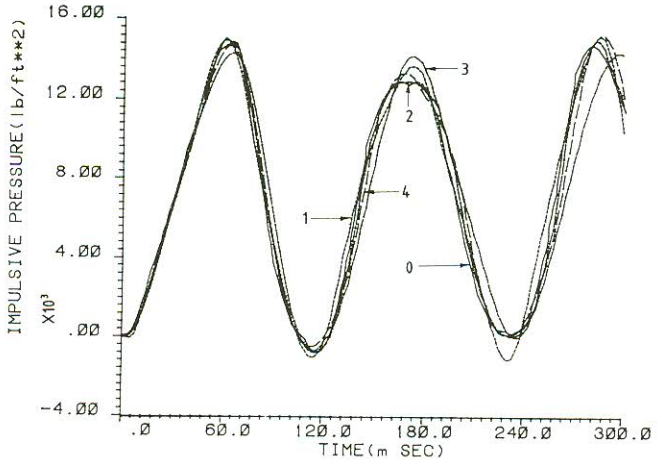

Figure 3d Reservoir under base motion. 0, Exact; 1, 4 node (implicit); 2, 8 node (implicit); 3, 4 node (explicit); 4, 8 node (explicit); $\Delta t=2.5$ msec (implicit cons.)

Chopra[11]. *Figure 3b* and *3c* show the impulsive pressure response (at $X=\gamma=30$ ft) for four-noded and eight-noded element 6×5 mesh integrated by implicit method with a time step of 2.5 msec. The results are compared with exact results[11] and numerical results[5] where results of direct integration (DI) and mode superposition (MS) are given by continuum mechanics approach. *Figure 3b* shows that present results trace the impulsive pressure response more accurately than that given in Reference 5. The phase shift and amplitude changes are the minimum for the present case. The results of eight-noded mesh in *Figure 3c* almost overlap the exact result within the accuracy of curve plotting.

Figure 3d compares four-node element and eight-node element results for implicit and explicit integration at a time step of 2.5 msec. It is noted that eight-node results (implicit and explicit cases) represent the pressure history very accurately, where calculation has been done at a time step close to the critical time step.

Exterior shell–fluid interaction problem

A spherical shell submerged in an infinite fluid medium and subjected to a step pressure is a classical problem of shell–fluid interaction. *Figure 4a* shows the details of this problem. Here the fluid

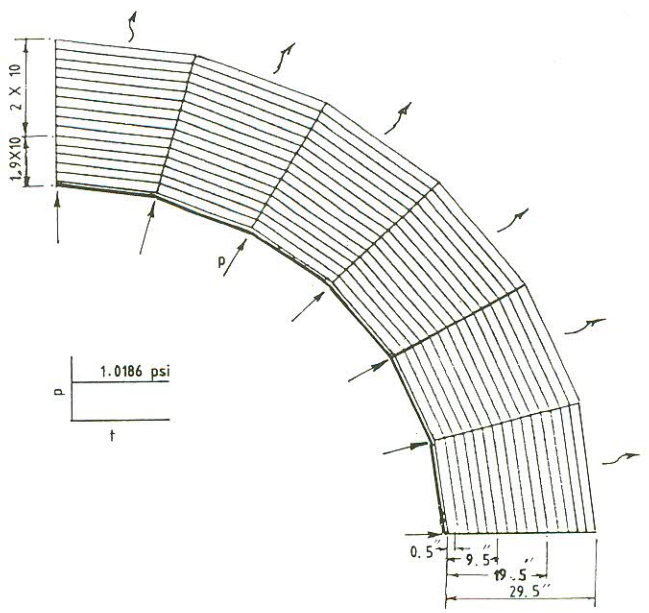

Figure 4a Spherical shell submerged in infinite fluid. Fluid: $\rho_f = 0.9582 \times 10^{-4}$ lb-s^2/in^4; $K = 3.33 \times 10^5$ lb/in^2. Shell: radius = 75 in; thickness = 1 in; $E = 29 \times 10^6$ lb/in^2; $\nu = 0.3$; $\rho_s = 7.345 \times 10^{-4}$ lb-s^2/in^4

mesh is taken up to a length of 29.5 in from the shell outer surface. A radiation boundary condition is specified at this end. In this problem the minimum time period for shell is an order of magnitude less than that of fluid. So one is again tempted to use *E–I* partitioning for fluid and shell meshes respectively. The critical time step for fluid is evaluated to be 0.033 msec, which is of the order of h/c ($h = 1.9$ in). For this problem also the number of iterations per time step is very large for *E–I* partitioning compared to *I–I* partitioning, as noted in the earlier problem of plate–fluid interaction. For example, the number of iterations were 20–25 for *E–I* partitioning compared to 5 to 6 iterations for *I–I* partitioning for a time step of 0.025 msec. Pressure wave propagation in fluid and radial shell deflection are shown in *Figures 4b* and *4c* for *E–I* partitioning and *Figures 4d* and *4e* for *I–I* partitioning respectively. For explicit solution of fluid mesh the radiation damping matrix $\mathbf{C}_f$ is lumped in the same manner as mass matrix $\mathbf{M}_f$. It is observed that if the time step is very close to the

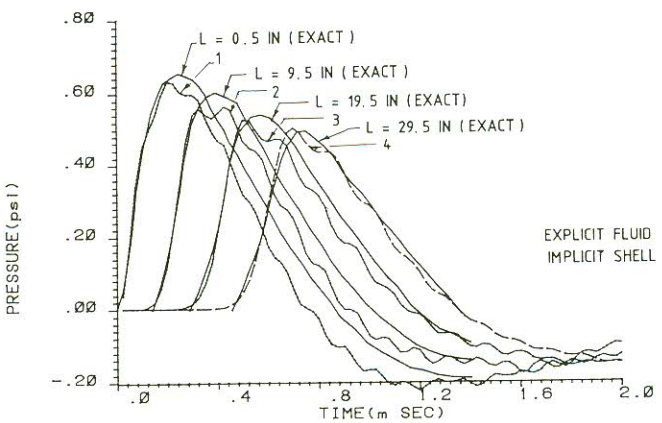

Figure 4b Pressure wave propagation from submerged sphere. $\Delta t = 0.025$ msec

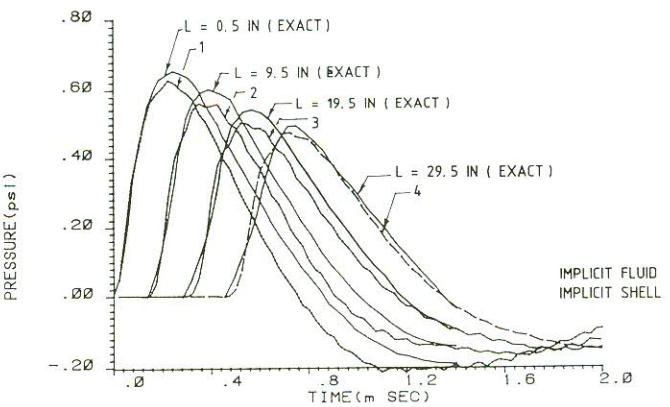

Figure 4d Pressure wave propagation from submerged sphere. $\Delta t = 0.025$ msec

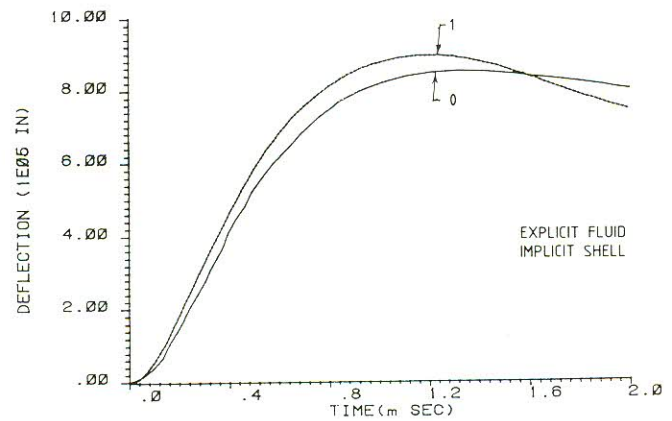

Figure 4c Radial deflection of submerged sphere. 0, Exact; 1, present; $\Delta t = 0.025$ msec

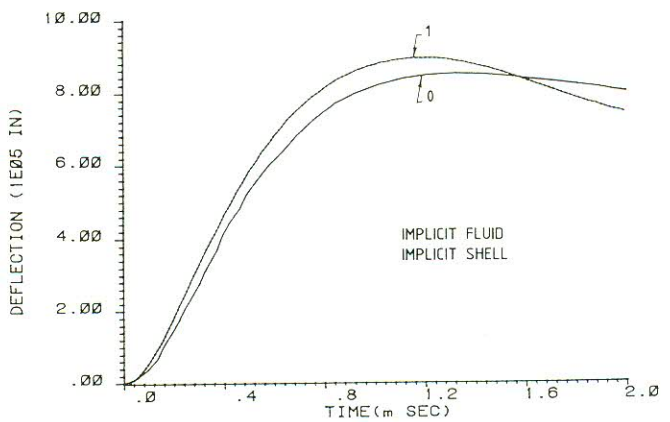

Figure 4e Radial deflection of submerged sphere. $\Delta t = 0.025$ msec. 0, Exact; 1, present

critical time step of fluid mesh, the convergence rate is slow and solution does not converge even after 100 iterations for a time step of 0.03 msec in *E–I* partitioning. *Figures 4f* and *4g* shows the results for a fully explicit calculation (*E–E*) for fluid and shell meshes respectively at a time step of 0.002 msec which is the critical time period for shell mesh.

In this problem the fluid oscillation is followed by shell vibration, so path 2 is the optimum. Path 3 is slightly slower than path 2 while path 1 is quite inefficient. For an *I–I* partitioning the convergence rate reduces with increase in time step up to 0.6 msec. Further increase in time step results in increased convergence rate (*Table 4*). This behaviour is similar to that noted for plate–fluid interaction problem. The time required for the wave to reach the end of fluid mesh is 0.5 msec. Here there is a transition from compressible to incompressible behaviour of fluid model due to temporal discretization.

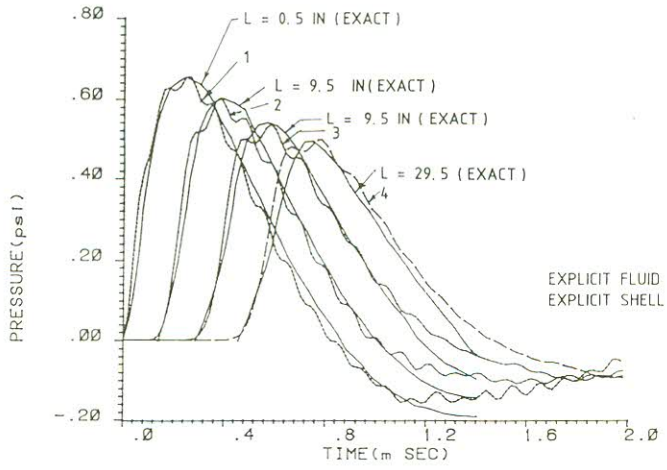

Figure 4f Pressure wave propagation from submerged sphere. $\Delta t = 0.002$ msec

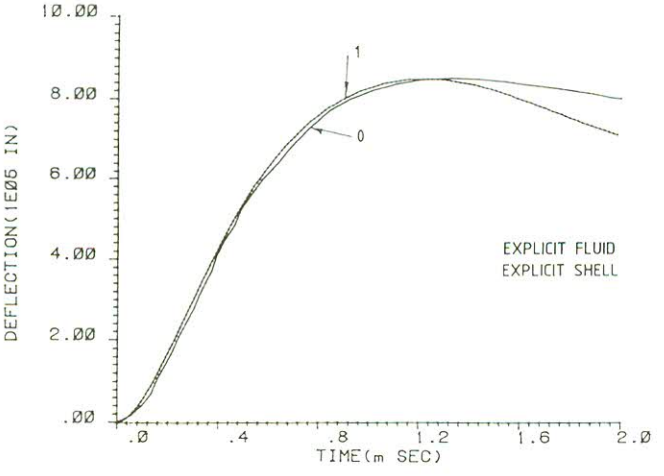

Figure 4g Radial deflection of submerged sphere. $\Delta t = 0.002$ msec. 0, Exact; 1, present

Interior shell-fluid interaction problem

Another problem used for study was of a spherical shell containing a fluid shown in *Figure 5a*. Here a thick spherical shell filled with a fluid was analysed for an impact pressure of 100 kg/cm^2 applied at outer shell pole. The pole pressure response is compared with results of References 5 and 6. The present results predict a very high pole pressure. The results at a radius of 6.5 in and at an angle of 5° from vertical axis (centre of pole element[5]) are close to the reported results as shown in *Figure 5b* for implicit integration with time steps of 2.5×10^{-3} msec and 3.125×10^{-4} msec. However, the present results show superposition of pressure waves in latter part of response after 0.2 msec. This is the time for the wave to reach back to the top pole after reflection from the lower pole which is not prominently depicted[5,6].

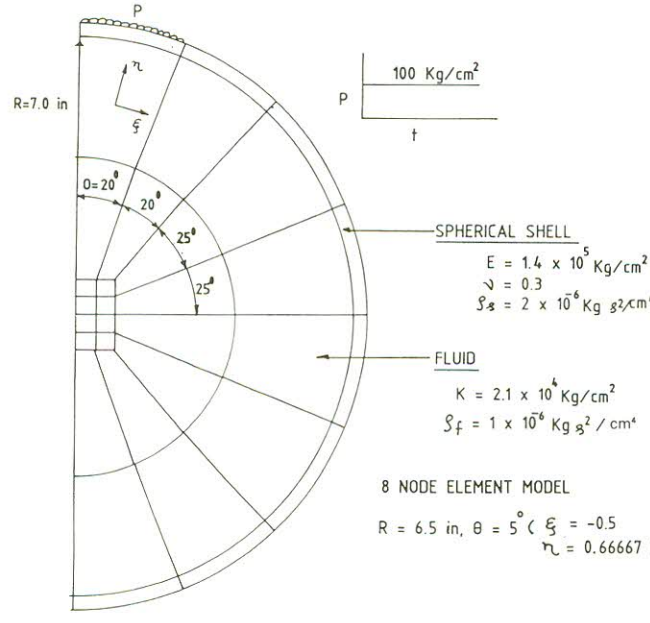

Figure 5a Interior shell–fluid interaction problem

Table 4 Number of iterations in computation path 2 for submerged spherical shell problem with *I–I* partitioning

	Compressible			Transition				Incompressible		
Time step (msec) →	0.01	0.08	0.1	0.5	0.6	0.8	1.0	2.0	5.0	10.0
Number of iterations	5	12	14	150	232	145	65	14	7	6

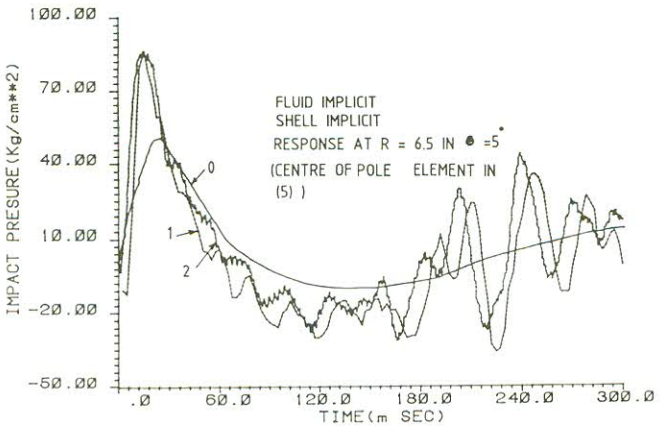

Figure 5b Interior shell–fluid interaction (8 node). 0, Ref. 6; 1, $\Delta t = 2.5 \times 10^{-3}$ msec; 2, $\Delta t = 3.125 \times 10^{-4}$ msec

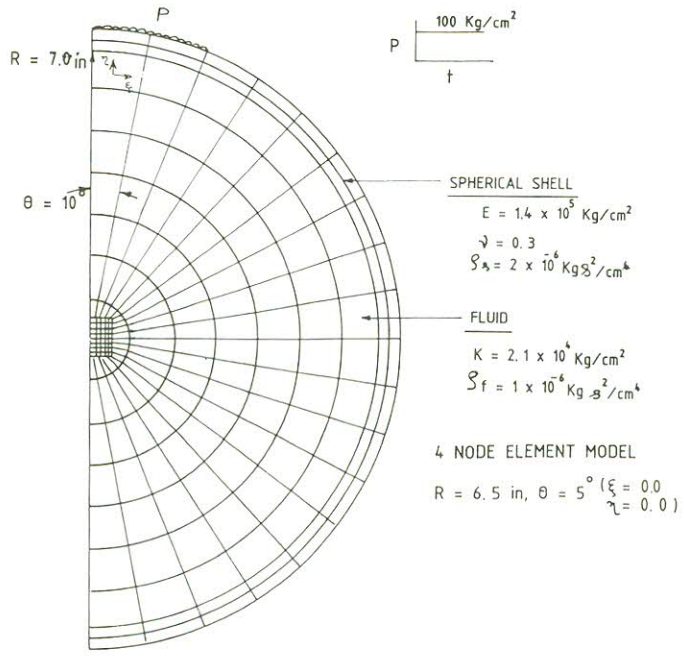

Figure 5c Interior shell–fluid interaction problem

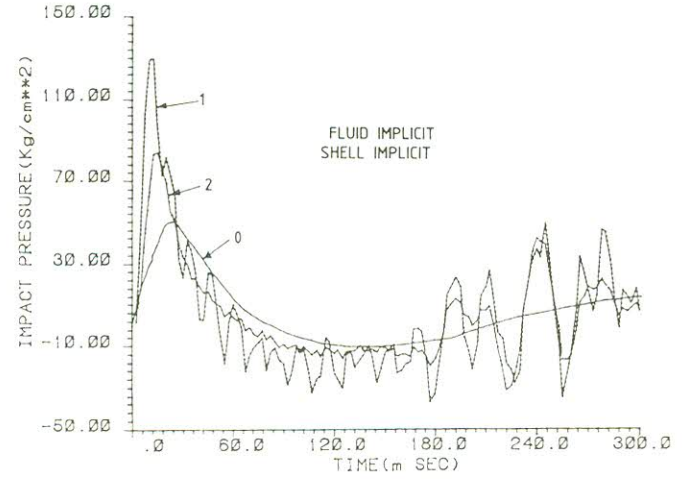

Figure 5d Interior shell–fluid interaction (4 node). 0, Ref. 6; 1, at pole; 2, at $R = 6.5$ in $\theta = 5°$; $\Delta t = 2.5 \times 10^{-3}$ msec

Further investigations were made with four-noded shell fluid mesh (*Figure 5c*). This is similar to the model used in Reference 5. *Figure 5d* shows the response at pole and at $R = 6.5$ in and at an angle of 5° from vertical axis (centre of pole element) for implicit integration with a time step of 2.5×10^{-3} msec. Again similar results are obtained as mentioned earlier with eight-noded elements. The two results are compared in *Figure 5e*. The problem was then analysed with a time step of 0.01 msec (same as that in Reference 5) for the four-noded element mesh with implicit integration. The results are shown in *Figure 5f*. Here it is clear that the present impact pressure at pole centre is in close agreement with that reported in Reference 5.

The critical time steps for four-noded element model are 3.0×10^{-4} msec and 8.7×10^{-4} msec for fluid and shell meshes respectively. Here time step size for explicit integration is governed by fluid domain. So at first an *E–E* partitioning for fluid

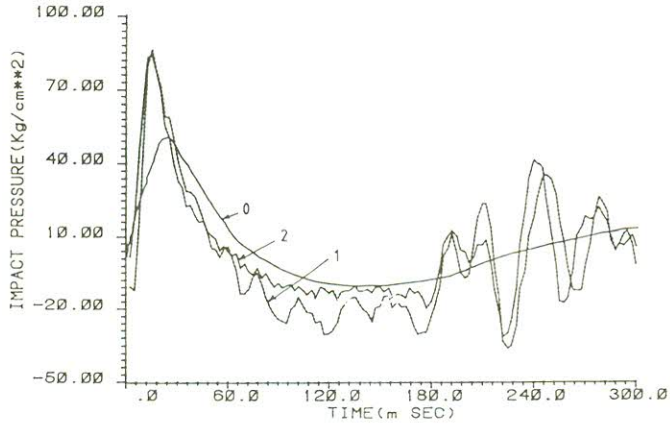

Figure 5e Interior shell–fluid interaction. 0, Ref. 6; 1, 8 node; 2, 4 node; $\Delta t = 2.5 \times 10^{-3}$ msec; response at $R = 6.5$ in $\theta = 5°$

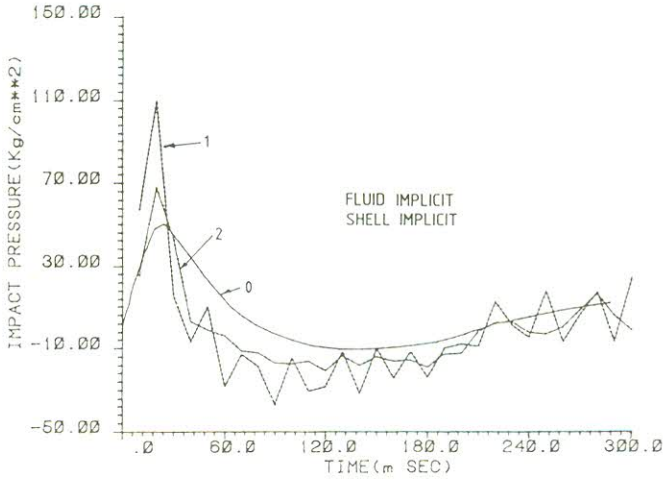

Figure 5f Interior shell–fluid interaction (4 node). 0, Ref. 6; 1, at pole; 2, at $R = 6.5$ in $\theta = 5°$; $\Delta t = 0.01$ msec

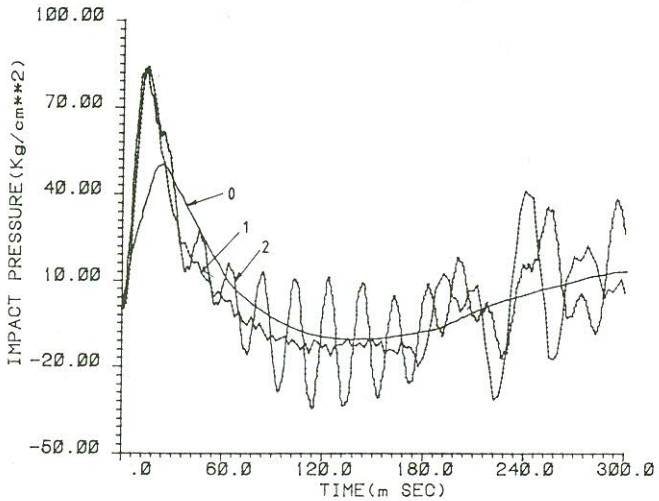

Figure 5g Interior shell–fluid interaction (4 node). 0, Ref. 6; 1, *I–I*, $\Delta t = 2.5 \times 10^{-3}$ msec; 2, *E–E*, $\Delta t = 3.0 \times 10^{-4}$ msec; response at $R = 6.5$ in $\theta = 5°$

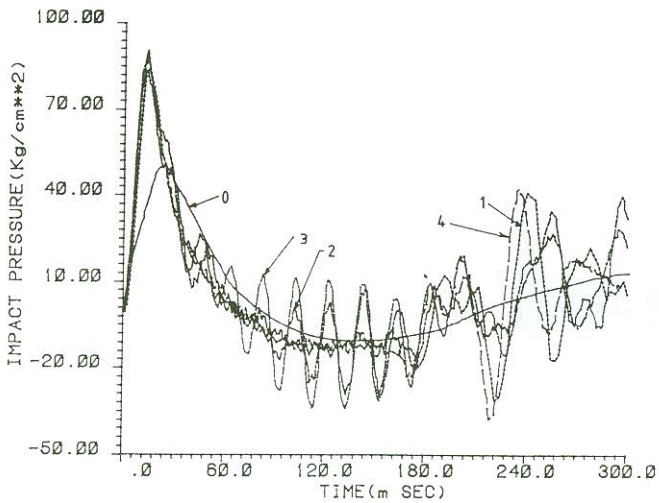

Figure 5h Interior shell–fluid interaction (4 node). 0, Ref. 6; 1, *I–I*, $\Delta t = 2.5 \times 10^{-3}$ msec; 2, *E–I–I*, $\Delta t = 8.2 \times 10^{-4}$ msec; 3, *E–I–E*, $\Delta t = 8.0 \times 10^{-4}$ msec; 4, *I–I*, $\Delta t = 8.0 \times 10^{-4}$ msec; response at $R = 6.5$ in $\theta = 5°$

and shell was made. The results with a time step of 3×10^{-4} msec are shown in *Figure 5g* where results of *I–I* partitioning with a time step of 2.5×10^{-3} msec are also shown. If the elements near the centre of fluid mesh are removed the critical time step for fluid is 8.2×10^{-4} msec. This suggests that *E–I* partitioning with the fluid mesh (implicit scheme for finer elements at centre) and explicit or implicit scheme for shell would be advantageous. *Figure 5h* shows the results for *E–I* fluid *I* shell partitioning with a time step of 8.2×10^{-4} msec and *E–I* fluid *E* shell partitioning with a time step of 8.0×10^{-4} msec. In the same Figure results of *I–I* partitioning for fluid and shell with time steps of 2.5×10^{-3} msec and 8×10^{-4} msec respectively are also shown for comparison. Here it may be noted that results of *E–E* and *E–I* partitionings show some oscillatory behaviour which is due to the spurious high frequency contribution. In pure implicit calculations (*I–I*) these spurious modes are not present.

The present results show different behaviour than reported elsewhere[5,6]. Further investigations were made by selecting damped Newmark algorithm ($\gamma = 0.6$ and $\beta = 0.3025$). This removes the effects of spurious mode but introduces some numerical damping. *Figure 5i* compares results of trapezoidal rule ($\gamma = 0.5$, $\beta = 0.25$) and damped Newmark algorithm for eight-node mesh with *I–I* partitioning. Similar comparison is made for four-node mesh in *Figure 5j*. These results also indicate the presence of reflected wave from lower pole at nearly 0.2 msec. For this problem also path 2 is the optimum one.

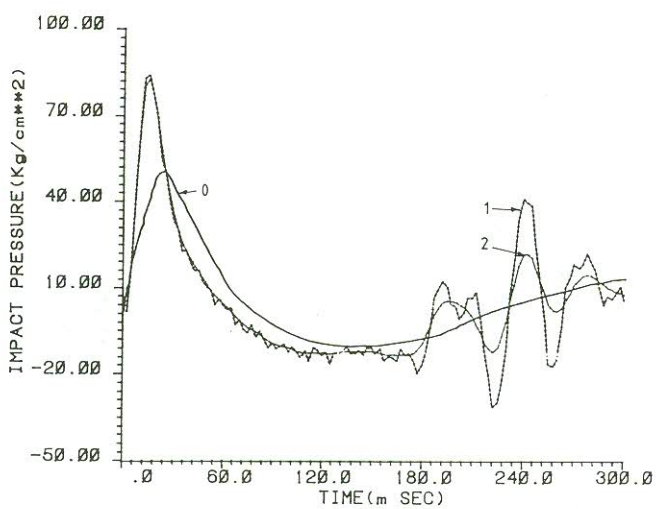

Figure 5i Interior shell–fluid interaction (8 node). 0, Ref. 6; 1, *I–I*, $\gamma = 0.5$, $\beta = 0.25$; 2, *I–I*, $\gamma = 0.6$, $\beta = 0.3025$; response at $R = 6.5$ in $\theta = 5°$

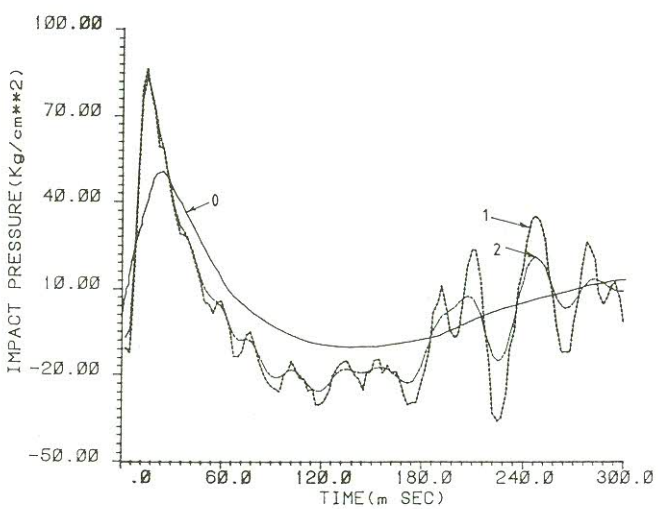

Figure 5j Interior shell–fluid interaction problem (4 node). 0, Ref. 6; 1, *I–I*, $\gamma = 0.5$, $\beta = 0.25$; 2, *I–I*, $\gamma = 0.6$, $\beta = 0.3025$; response at $R = 6.5$ in $\theta = 5°$

CONCLUSIONS

It is found that based on the stability criteria for numerical integration of single field problems, time step estimates could be made for coupled field problems if minimum time period estimates are available for individual fields. For *E–I* partitioning there is a small reduction in the time step (of about 10 to 20% of Δt_{cr}) from convergence requirement. This is of the same order as reported by Belytschko[10] for non-linear problems, since in the present case also the interaction term may be regarded analogous to pseudo force term of non-linear dynamic problems. *E–I* partitioning could be exploited for problems where fluid minimum time period is larger then structure minimum period (this is often the case in many problems). Again individual fields also could be further partitioned if they have some stiff elements (either due to material properties or due to finer discretization). This has been demonstrated in problem 5. For problems where structure first transfers load to fluid path 2 (structure then fluid) is useful. In this after the predictor phase, correction is made in structure response in Newmark predictor–multi-corrector integration scheme. For problems of wave propagation in fluid where a pressure pulse in fluid moves and transfers load to structure path 3 (fluid then structure) is useful.

Although *I–I* partitioning is costly in terms of the time required for solution of equations, nevertheless the number of iterations for convergence per time step is small. Thus this method could also be exploited since only the accuracy and convergence requirements are to be met for this type of partitioning. The characteristic of unconditional stability is retained up to a very large time step for coupled problems also if correct computational path is selected. Time step estimate for fully implicit calculation could be made in such a manner that numerical model gives compressible solution. This can be easily estimated from characteristic length of fluid structure system. The optimum choice between *E–I* and *I–I* partitioning will depend on the order of time steps for fluid and structure meshes.

In staggered scheme the representation of shock fronts, pressure transients are more accurate compared to continuum mechanics approach and reliable structure response is also obtained. This methodology is very well suited for modular adoption for a variety of coupled linear and non-linear fluid and structure problems in parallel processing environment.

APPENDIX I

Fluid domain Ω_f

Pressure in the element is given by shape function N_f and nodal pressure $\mathbf{p}$ by:

$$p = \mathbf{N}_f \mathbf{p} \tag{I.1}$$

Fluid element mass matrix is:

$$(M_f^e)_{ij} = 1/c^2 \int_{\Omega_f} N_{fi}^{\mathrm{T}} N_{fj} + 1/g \int_{\Gamma_F} N_{fi}^{\mathrm{T}} N_{fj} \, \mathrm{d}\Gamma_F \tag{I.2}$$

Fluid element radiation damping matrix is:

$$(C_f^e)_{ij} = 1/c \int_{\Gamma_R} N_{fi}^{\mathrm{T}} N_{fj} \, \mathrm{d}\Gamma_R \tag{I.3}$$

Fluid element stiffness matrix is:

$$(K_f^e)_{ij} = \int_{\Omega_f} (N_{fi}, xN_{fj}, x + N_{fi}, yN_{fj}, y) \, \mathrm{d}\Omega_f \tag{I.4}$$

Structure domain Ω_s

Displacement $\boldsymbol{\delta}$ in the element is given by shape function $\mathbf{N}_s$ and nodal displacement $\mathbf{u}$:

$$\boldsymbol{\delta} = N_s \mathbf{u} \tag{I.5}$$

Structure element mass matrix is:

$$(M_s^e)_{ij} = \int_{\Omega_s} \rho_s N_{si}^{\mathrm{T}} N_{sj} \, \mathrm{d}\Omega_s \tag{I.6}$$

where ρ_s is the mass density of structure element.

Structure element stiffness matrix is:

$$(K_s^e)_{ij} = \int_{\Omega_s} B_{im} D_{mk} B_{kj} \, \mathrm{d}\Omega_s \tag{I.7}$$

where $\mathbf{B}$ and $\mathbf{D}$ are strain displacement matrix and constitutive law matrix respectively. These are given in References 15 and 16.

The structure damping matrix is obtained by:

$$\mathbf{C}_s = a\mathbf{M}_s + b\mathbf{K}_s \tag{I.8}$$

where a and b are constants to control damping proportionately.

Coupling matrix at fluid structure interface is:

$$\mathbf{Q}_s = \int_{\Gamma_I} \mathbf{N}_s^{\mathrm{T}} \hat{n} \mathbf{N}_f \, \mathrm{d}\Gamma_I \tag{I.9}$$

where $\hat{n}$ gives unit normal components at fluid structure interface.

APPENDIX II

Predictor–multi-corrector algorithm for semi-discrete coupled second-order equations[3,14]

Second-order equation[1] at time step $n+1$ is given as:

$$\mathbf{M}\ddot{\mathbf{u}}_{n+1}+\mathbf{C}\dot{\mathbf{u}}_{n+1}+\mathbf{K}\mathbf{u}_{n+1}=\mathbf{F}^2_{n+1} \tag{II.1}$$

$$i=0 \qquad (i=\text{iteration count}) \tag{II.2}$$

$$\left.\begin{aligned}\mathbf{u}^i_{n+1}&=\tilde{\mathbf{u}}_{n+1} &\text{(II.3)}\\ \dot{\mathbf{u}}^i_{n+1}&=\tilde{\dot{\mathbf{u}}}_{n+1} &\text{(II.4)}\\ \ddot{\mathbf{u}}^i_{n+1}&=\mathbf{0} &\text{(II.5)}\end{aligned}\right\}\text{predictor phase}$$

where

$$\tilde{\dot{\mathbf{u}}}_{n+1}=\dot{\mathbf{u}}_n+\Delta t(1-\gamma)\ddot{\mathbf{u}}_n \tag{II.6}$$

$$\tilde{\mathbf{u}}_{n+1}=\mathbf{u}_n+\Delta t\dot{\mathbf{u}}_n+\tfrac{1}{2}\Delta t^2(1-2\beta)\ddot{\mathbf{u}}_n \tag{II.7}$$

γ and β are Newmark's parameters, Δt is the time step.

Notes

1. Subscript is dropped as it may be used for any field.
2. The force augments applied force, specified boundary condition and interaction term.
3. $\gamma \geqslant \frac{1}{2}$, $\beta=(\gamma+\frac{1}{2})^2/4$ leads to unconditional stability for single pass single field problem.
4. Mesh partitioning is possible by recognizing elements either as explicit or as implicit:

$$\mathbf{M}=\mathbf{M}^I+\mathbf{M}^E \tag{II.15}$$

$$\mathbf{C}=\mathbf{C}^I+\mathbf{C}^E \tag{II.16}$$

$$\mathbf{K}=\mathbf{K}^I+\mathbf{K}^E \tag{II.17}$$

$$\mathbf{F}=\mathbf{F}^I+\mathbf{F}^E \tag{II.18}$$

and modifying the governing (II.1) as:

$$\mathbf{M}^I\ddot{\mathbf{u}}_{n+1}+\mathbf{M}^E\ddot{\mathbf{u}}_{n+1}+\mathbf{C}^I\dot{\mathbf{u}}_{n+1}+\mathbf{K}^I\mathbf{u}_{n+1}=\mathbf{F}^I_{n+1}+\mathbf{F}^E_{n+1} \tag{II.19}$$

$$\left.\begin{aligned}\mathbf{K}^*\Delta\mathbf{u}^i&=\mathbf{f}^{*i}_{n+1} &\text{(II.8)}\\ \mathbf{K}^*&=\mathbf{M}/\beta\Delta t^2+\gamma\mathbf{C}/\beta\Delta t+\mathbf{K} &\text{(II.9)}\\ \mathbf{f}^{*i}_{n+1}&=\mathbf{F}^i_{n+1}-\mathbf{M}\ddot{\mathbf{u}}^i_{n+1}-\mathbf{C}\dot{\mathbf{u}}^i_{n+1}-\mathbf{K}\mathbf{u}^i_{n+1} &\text{(II.10)}\end{aligned}\right\}\text{solution phase}$$

$$\left.\begin{aligned}\mathbf{u}^{i+1}_{n+1}&=\mathbf{u}^i_{n+1}+\Delta\mathbf{u}^i &\text{(II.11)}\\ \ddot{\mathbf{u}}^{i+1}_{n+1}&=(\mathbf{u}^{i+1}_{n+1}-\tilde{\mathbf{u}}_{n+1})/\beta\Delta t^2 &\text{(II.12)}\\ \dot{\mathbf{u}}^{i+1}_{n+1}&=\dot{\mathbf{u}}^i_{n+1}+\gamma\Delta t\ddot{\mathbf{u}}^{i+1}_{n+1} &\text{(II.13)}\end{aligned}\right\}\text{corrector phase}$$

Check convergence $\|\Delta\mathbf{u}^i\|/\|\mathbf{u}^{i+1}\| \leqslant \text{Tolerance}$ (II.14)

$i \rightarrow i+1$ NO

YES

$n \rightarrow n+1$ and go to (II.2) for next time step.

5. Lumping of **M** is done by special lumping technique[15].

REFERENCES

1 Au-Yang, M. K. and Galford, J. E. Fluid–structure interaction—a survey with emphasis on its application to nuclear steam system design, *Nucl. Eng. Design*, **70**, 387–399 (1982)

2 Park, K. C. and Felippa, C. A. Partitioned analysis of coupled systems, in *Computational Methods for Transient Analysis* (Eds. T. Belytschko and T. J. R. Hughes), North-Holland, Amsterdam, Ch. 4 (1983)

3 Paul, D. K. Single and coupled multifield problems, *PhD Thesis*, University College of Swansea (1982)

4 Felippa, C. A. and Geers, T. L. Partitioned analysis for coupled mechanical systems, *Eng. Comput.*, **5**, 123–133 (1988)

5 Akkas, N., Akay, H. U. and Yilmaz, C. Applicability of general purpose finite element programmes in solid–fluid interaction problems, *Comp. Struct.*, **10**, 773–783 (1979)

6 Shugar, T. A. and Katona, M. G. Development of finite element head injury model, *J. Eng. Mech. Div., ASCE*, **EMS-101**, 223–239 (1975)

7 Wilson, E. L. and Khalvati, M. Finite elements for the dynamic analysis of fluid–solid systems, *Int. J. Num. Meth. Eng.*, **19**, 1657–1668 (1983)

8 Bathe, K. J. and Hahn, W. F. On treatment analysis of fluid–structure systems, *Comp. Struct.*, **10**, 383–391 (1979)

9 Liu, W. K. and Chang, H. G. A method of computation for fluid structure interaction, *Comp. Struct.*, **20**, 311–320 (1985)

10 Belytschko, T. Fluid–structure interaction, *Comp. Struct.*, **12**, 459–469 (1980)

11 Chopra, A. K., Wilson, E. L. and Farhoomand, I. Earthquake analysis of reservoir dam systems, *Proc. 4th World Conf. Earthquake Engineering, Santiago, Chile, 1969*

12 Chakrabarti, P. and Chopra, A. K. Earthquake response of gravity dams including reservoir interaction effects, *EERC 72-6*, University of California, Berkeley (1972)
13 Belytschko, T. and Hughes, T. J. R. (Eds.). *Computational Methods for Transient Analysis*, North-Holland, Amsterdam (1983)
14 Hughes, T. J. R. *The Finite Element Method*, Prentice-Hall, Englewood Cliffs, NJ (1987)
15 Owen, D. R. J. and Hinton, E. *Finite Elements in Plasticity: Theory and Practice*, Pineridge Press, Swansea (1980)
16 Zienkiewicz, O. C. *The Finite Element Method*, 3rd Edn., McGraw-Hill, London (1976)
17 Newmark, N. M. and Rosenblueth, E. *Fundamentals of Earthquake Engineering*, Prentice-Hall, Englewood Cliffs, NJ (1971)
18 Singh, R. K., Kakodkar, A. and Kant, T. Some studies on fluid structure interaction problems, *Report No. BARC-1424*, BARC, Trombay, Bombay (1988)
19 Shantaram, D., Owen, D. R. J. and Zienkiewicz, O. C. Dynamic transient behaviour of two or three dimensional structures, including plasticity, large deformation effects and fluid interaction, *Earthqu. Eng. Struct. Dyn.*, **4**, 561–576 (1976)
20 Liu, W. K. Development of finite element procedures for fluid structures interaction, *PhD Thesis*, *EERL 80-86*, California Institute of Technology, University of California, Berkeley (1981)
21 Geers, T. L. and Ruzicka, C. Finite element/boundary-element analysis of multiple structures excited by transient acoustic waves, in *Numerical Methods for Transient and Coupled Problems* (Eds. R. W. Lewis, P. Bettess and E. Hinton), Pineridge Press, Swansea, pp. 150–162 (1984)
22 Schreyer, H. L. Dispersion of semidiscretized and fully discretized systems, in *Computational Methods for Transient Analysis* (Eds. T. Belytschko and T. J. R. Hughes), North-Holland, Amsterdam, Ch. 6 (1983)
23 Belytschko, T. A survey of numerical methods and computer programs for dynamic structural analysis, *Nucl. Eng. Design*, **37**, 23–24 (1976)
24 Belytschko, T. and Mullen, R. Stability and explicit–implicit mesh partitions in time integration, *Int. J. Num. Meth. Eng.*, **12**, 1575–1986 (1978)
25 Belytschko, T., Yen, H. J. and Mullen, R. Mixed methods for time integration, *Comp. Meth. Appl. Mech. Eng.*, **17/18**, 259–275 (1979)

Automatic crack propagation studies in T-junctions and cross bars

E. M. Remzi
Information Technology Dept, PowerGen PLC, 85 Park Street, London SE1 9DY, UK

and W. S. Blackburn
Gravesend Laboratories, Nuclear Electric PLC, Gravesend, UK
(Received January 1989)

ABSTRACT

Theoretical investigations have been performed on slowly propagating cracks in T-junctions and cross bars using computer procedures developed to analyse the amount and direction of crack growth using automatic mesh modification and the finite element stress analysis program, BERSAFE. The procedures may be used in a linear or non-linear material. The crack growth for the linear elastic case is calculated to be in the direction of the maximum energy release rate. For the non-linear case, the direction is taken to be that of $J^*_{w_i}$. These procedures have been applied to fatigue crack growth calculations in this paper.

INTRODUCTION AND BACKGROUND

Numerical modelling of fracture processes is an area which has seen many advances recently. These advances have provided effective and accurate ways of evaluating fracture parameters for assessing the integrity of structures containing defects. For example, the repair or replacement of defective structures can be avoided if it can be shown that defects will not grow in service. The simulation of crack propagation can also be approached more effectively using these parameters. The main concern is then to predict how long the component will operate safely under service conditions.

Suitable parameters for characterizing the amount and direction of crack growth in a non-linear material are the components of contour integrals (J)[1,2] around crack tips. When non-linear effects are unimportant their values are simply related to the stress intensity factor, K. Energy methods such as the virtual crack extension techniques[3–5] are also well established.

An extensive review of the contour integrals has been given by Hellen and Blackburn[6]. A numerically robust integral which has a wide range of validity is:

$$J^*_{w_i} = \int \left(W \, \mathrm{d}x_2 - T_i \frac{\partial u_i}{\partial x_1} \, \mathrm{d}s \right) \tag{1}$$

for a small contour around the crack where:

(x_1, x_2) = coordinates along and perpendicular to the crack plane,
u_i = components of displacement,
T_i = components of tractions,

and for stresses, σ_{ij} and strains, ε_{ij} related by the strain energy potential W, where

$$\sigma_{ij} = \frac{\partial W}{\partial \varepsilon_{ij}} \tag{2}$$

This may be evaluated on other contours as a contour integral plus a surface integral over the area between[6].

Catalogued procedures called BERCRAG[7] have been developed to analyse the growth of a crack using automatic mesh modification and the finite element stress analysis program BERSAFE[8]. Using these procedures calculations of the direction of crack growth have been performed on slowly propagating cracks in T-junctions and cross bars. Displacement conditions were imposed to produce tensile loading on the base and bending on the arm. Crack propagation paths were predicted for a number of initial crack orientations and sizes for varying tension to bending ratios for the linear elastic case. A smaller number of cases have also been analysed for a non-linear material.

BERCRAG

Automatic mesh modification programs were written to modify a two-dimensional or axisymmetric mesh containing a crack with four quadrilateral elements around the tip by allowing for slow crack growth. These were also extended to three-dimensional meshes with a crack on its boundary representing a plane of symmetry.

The procedures may be used for a crack in a linear or non-linear material. In a linear elastic material, the crack growth is usually due to fatigue. For non-linear materials, three different crack laws are available; fatigue, creep and ductile tearing. A further option is also available where the combined

0264-4401/90/020116-11$2.00